Journal of Science and Transport Technology
Journal homepage: https://jstt.vn/index.php/en

Seismic Response and Frequency Degradation of Low-Rise RC Shear Walls: A Validated Nonlinear Model for Nuclear Structures

Khuong Le Nguyen[1], Cao Minh Quyen[2]*, Khuyen Truong Manh[3]
[1]Building & Construction Management at the School of Design and Built Environment, University of Canberra, Australia
[2]Advanced Materials and Intelligent Systems for Infrastructure and High-Speed Rail (AMIS-HSR) research group, University of Transport Technology, Hanoi, Vietnam
[3]Faculty of Civil Engineering, Hanoi Architectural University, Hanoi, Vietnam

Article info
Type of article:
Original research paper

DOI:
https://doi.org/10.58845/jstt.utt.2025.en.5.4.294-316

***Corresponding author:**
Email address:
quyencm@utt.edu.vn

Received: 27/09/2025
Received in Revised Form: 26/11/2025
Accepted: 18/12/2025

Abstract: Reinforced concrete (RC) shear walls are key seismic-resisting components in nuclear facilities, where reliable prediction of stiffness and damage under strong ground motion is critical. The evolution of natural frequency with damage is central to performance assessment and structural health monitoring. This paper validates a mesh-regularized nonlinear finite element model of low-rise RC shear walls with explicit focus on seismic response and frequency degradation relevant to nuclear structures. Four walls from the SAFE/CASH international benchmark program (T6, T7, T8, T9), sharing identical geometry but different axial load levels (0.2 MPa and 1.8 MPa) and horizontal reinforcement ratios (0.5% and 1.0%), are analyzed under three loading protocols: monotonic pushover, quasi-static cyclic, and pseudo-dynamic tests conducted at the ELSA laboratory. Concrete is represented by a smeared-crack model with fracture-energy regularization following the Hillerborg approach, and reinforcement by an embedded steel model with a cyclic Menegotto-Pinto constitutive law. The model accurately reproduces base-shear-drift envelopes and the dominant trend of frequency drop for all four walls, predicting peak strength within 2% error and frequency degradation within 10-15% of experimental values. However, it consistently underestimates cumulative hysteretic energy dissipation by up to 30% in high-axial-load cases (T7 and T9), indicating a conservative bias in energy absorption prediction. These results quantify both the reliability and limitations of a 2D smeared-crack approach for nuclear-type shear walls and provide practical recommendations on optimal mesh size, calibration strategy based on material test data, and the interpretation of frequency-based damage indicators for structural health monitoring in nuclear engineering applications.

Keywords: RC shear walls, nonlinear finite element analysis, seismic response, frequency degradation, nuclear structures, model validation, smeared crack model.

1. Introduction

Reinforced concrete (RC) shear walls are fundamental structural elements for resisting lateral loads in safety-critical facilities, most notably in Nuclear Power Plants (NPPs) [1, 2, 3]. Their high in-plane stiffness and strength make them the primary line of defense against seismic events [4, 5]. The robust performance of these walls is paramount to ensure nuclear safety, both during and after an earthquake. Consequently, accurately predicting their nonlinear behavior, damage progression, and residual capacity under strong ground motion is a central challenge in the seismic design and assessment of NPPs [4, 6, 7].

Over the past decades, significant research has been dedicated to understanding and modeling the complex behavior of RC shear walls. Experimental campaigns, such as the CAMUS [8] and pseudo-dynamic benchmarks [2, 3], have provided invaluable data on their response. Numerical modeling has evolved from simplified macro-models to sophisticated finite element (FE) approaches. These FE models can be broadly categorized into discrete crack models, which represent cracks as distinct discontinuities, and smeared crack models, which average the cracking behavior over a finite element volume [9, 10, 11]. While discrete models can capture localized fracture with high fidelity, smeared crack models are often more practical for large-scale structural analysis due to their computational efficiency and simpler mesh requirements [10, 12].

However, a persistent challenge with smeared crack models is their pathological mesh sensitivity, where the predicted response changes with the size of the finite elements. To address this, fracture energy regularization techniques, pioneered by Hillerborg et al. [9], have been introduced. These methods ensure that the energy dissipated during fracture is independent of the mesh size, leading to more objective and reliable results [9, 11].

While the prediction of force-displacement capacity (i.e., the "backbone curve") has been the focus of many validation studies [4, 5, 13], the evolution of dynamic properties, such as the structure's natural frequency, has received less attention. The degradation of natural frequency is a direct physical manifestation of accumulated damage and stiffness loss [5, 14, 15]. For nuclear facilities, which are increasingly being equipped with Structural Health Monitoring (SHM) systems, tracking frequency shifts provides a powerful, non-intrusive method for post-earthquake damage assessment. A numerical model that can accurately predict this frequency degradation is therefore not just a design tool, but a critical component of a modern monitoring and assessment framework.

This paper aims to bridge this gap by presenting a comprehensive validation of a 2D nonlinear FE model based on a smeared-crack approach with fracture-energy regularization. The model is specifically tailored for the analysis of low-rise, squat shear walls typical of nuclear structures. The validation is performed against a rich experimental dataset from pseudo-dynamic and cyclic testing programs of RC shear walls [2, 3, 8].

The primary objectives of this study are threefold:

To quantify the accuracy of a practical, engineering-oriented FE model in predicting not only the global force-displacement response but also the detailed frequency degradation of nuclear-type shear walls.

To characterize any systematic biases in the model, particularly concerning energy dissipation, and discuss their implications for nuclear safety assessment.

To establish a robust and practical modeling strategy, including recommendations for mesh size and calibration, that can be confidently applied in the seismic analysis of nuclear structures.

To demonstrate the direct relevance of frequency-based validation metrics for addressing practical challenges of seismic safety assessment and structural health monitoring in nuclear facilities.

2. The SAFE/CASH Experimental Program

The experimental basis for this validation study comprises pseudo-dynamic and cyclic tests conducted on large-scale reinforced concrete shear walls [2, 3]. The tests were performed at the European Laboratory for Structural Assessment (ELSA) at the Joint Research Centre (JRC) in Ispra, Italy [2], as part of a broader international research effort to investigate the beyond-design seismic capacity of low-rise RC shear walls representative of those found in nuclear facilities [3, 8].

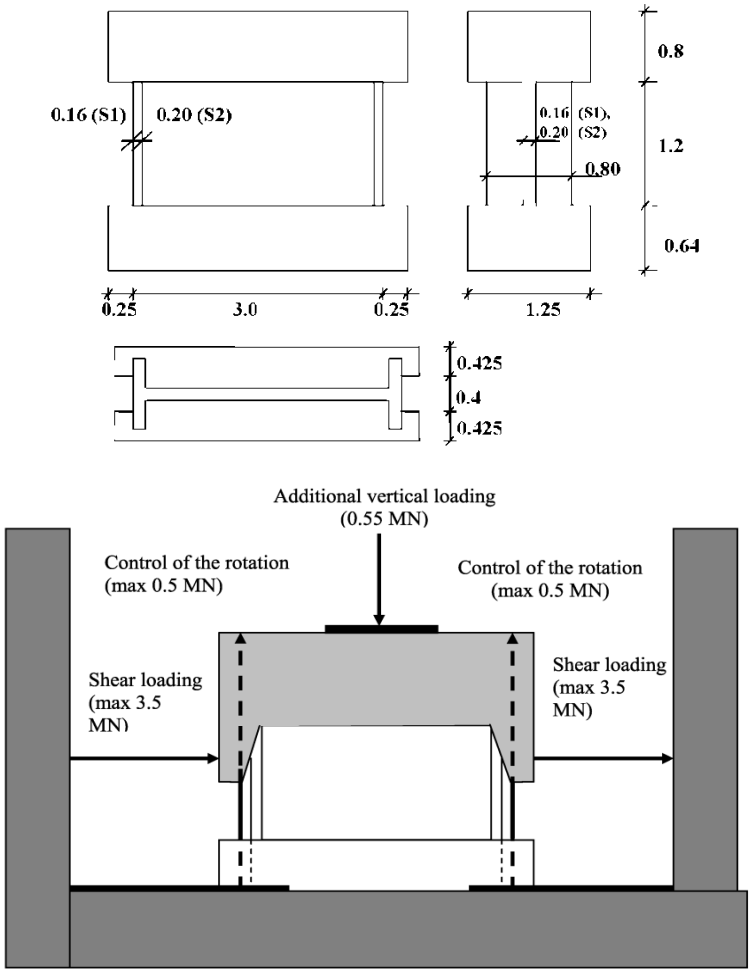

Fig. 1. Geometry of the wall (unit in m) and the test setup

Table 1. Main characteristics of the four SAFE shear walls

		T6	T7	T8	T9
Vertical reinforcement ratio	$\rho_v[\%]$	0.4	0.4	0.4	0.4
Horizontal reinforcement ratio	$\rho_h[\%]$	0.6	0.6	0.4	0.4
Confinement stress	$\sigma_n[MPa]$	1	1	0.34	0.34
Measured natural frequency at the start of the test	$f_0[Hz]$	10.4	3.6	9.6	2.9
Numerical mass to calibrate to the design frequency	$m[t]$	1252	11272	1252	11272

2.1. Test Specimens

Four large-scale RC shear walls, designated T6, T7, T8, and T9, were selected for this validation study. All four specimens shared identical geometry: a height of 1.2 m, a length of 3.0 m, and a thickness of 0.2 m, resulting in a squat aspect ratio (height-to-length ratio) of 0.4. This low aspect ratio is characteristic of shear walls in Nuclear

Power Plants, which are specifically designed to resist lateral loads through shear mechanisms while maintaining high stiffness and limited ductility demands [3-5]. The squat configuration ensures that the walls are governed by shear rather than flexural deformation modes, which is critical for nuclear safety considerations. A schematic of the wall geometry and reinforcement detailing is shown in Fig. 1.

The primary variables investigated across the four specimens were the level of applied axial compressive load and the amount of horizontal (transverse) reinforcement, as summarized in Table 1. Walls T6 and T8 were subjected to a low axial load (0.2 MPa), while T7 and T9 were subjected to a high axial load (1.8 MPa), representing different loading conditions within a nuclear structure, with the high axial load simulating upper stories of multi-story shear wall buildings. The horizontal reinforcement ratio varied between 0.6% (T6, T7) and 0.4% (T8, T9), allowing for an investigation of the influence of confinement and shear resistance on the seismic response. This parametric variation enables examination of two key effects: (1) the influence of axial load on shear capacity, ductility, and energy dissipation (comparing T6 vs T7 and T8 vs T9), and (2) the effect of horizontal reinforcement on crack control and post-peak behavior (comparing T6 vs T8 and T7 vs T9). All walls maintained constant vertical reinforcement ratio of 1.0%.

2.2. Material Properties

The material properties were characterized through comprehensive testing conducted as part of the experimental program. The concrete exhibited a mean compressive strength (f'c) of 43.4 MPa measured on 150 mm cubes at 28 days, and a mean tensile strength (ft) of 3.32 MPa. The longitudinal and transverse steel reinforcement bars demonstrated yield strengths (fy) ranging from 558 MPa to 601 MPa and ultimate strengths (fu) from 649 MPa to 682 MPa, depending on the bar diameter [2, 3]. These material properties are representative of high-quality concrete and high-strength steel reinforcement typically specified for nuclear safety-related structures.

2.3. Loading Protocols

The walls were subjected to a series of demanding loading protocols to comprehensively assess their seismic performance:

Monotonic Pushover: A slow, monotonically increasing horizontal displacement was applied to the top of the wall to determine its ultimate capacity and force-displacement envelope.

Quasi-Static Cyclic: A series of displacement-controlled cycles with increasing amplitude were applied to investigate the hysteretic behavior, stiffness degradation, and energy dissipation characteristics of the walls.

Pseudo-Dynamic (PsD): This advanced hybrid simulation technique [1] was employed to subject the physical specimens to realistic seismic loading conditions. In the PsD method, the equation of motion for the structure is solved numerically in real-time by a control system, which calculates the displacement to be imposed on the specimen through servo-controlled hydraulic actuators [1, 2]. The restoring forces measured from the specimen are then fed back to the numerical integration algorithm to compute the next displacement increment. This approach effectively couples physical testing with numerical time integration, enabling the evaluation of large-scale structural components under realistic earthquake ground motions without requiring an excessively large shaking table [1]. The PsD tests consisted of a sequence of seismic runs with systematically increasing intensity levels [3, 8]. The input ground motion was an artificial accelerogram compatible with response spectra representative of design basis earthquake scenarios for nuclear facilities, ensuring relevance to the seismic safety assessment of NPPs [3].

3. Numerical Modeling Approach

The numerical simulations were performed using the CAST3M finite element code developed by the French Alternative Energies and Atomic Energy Commission (CEA) [16]. The modeling

strategy was designed to balance physical representativeness with computational efficiency, making it suitable for large-scale structural analyses of nuclear facilities.

3.1. Finite Element Discretization

A two-dimensional (2D) plane stress formulation was adopted for the analysis. The concrete wall was discretized using four-node quadrilateral elements with bilinear interpolation functions. To investigate and mitigate potential mesh sensitivity effects—a primary objective of this study—three different uniform mesh sizes were systematically examined: coarse mesh (element size h = 20 cm), medium mesh (h = 10 cm), and fine mesh (h = 5 cm).

The steel reinforcement was represented using two-node bar elements embedded within the concrete elements. A perfect bond condition was assumed between concrete and steel, which is a standard assumption in macro-scale finite element analysis where local bond-slip effects are implicitly incorporated through the material constitutive models, particularly via the tension stiffening representation in the concrete model [9, 12, 17].

3.2. Constitutive Models

The nonlinear structural response is governed by the constitutive laws assigned to the concrete and steel materials, as described in the following subsections.

3.2.1. Smeared Crack Model with Fracture Energy Regularization

The concrete INSA model has 5 main parameters. The Young's modulus, the tensile strength and the ultimate compressive stress are determined by tests. We still have to determine two important parameters: the plastic strain at failure in compression, and especially the plastic strain at failure in tension which plays an essential role since it controls the development of cracking. After the peak of compression or tension, the behavior becomes softening, which makes the results sensitive to the mesh size. In order to guarantee a certain objectivity of the results, particularly with regard to the overall results, a classical regularization technique is adopted, known as the Hillerborg approach [13], based on the fracture energy in tension or the fracture energy in compression. The plastic strain parameters at failure in tension and in compression become dependent on these energies, considered as intrinsic to the material, as well as on a characteristic length obtained from the mesh and the type of finite element. The calculation procedures for the failure strains are detailed below.

Plastic Strain at Failure in Compression:

The identification of this parameter requires a complete uniaxial compression test, controlled in displacement. This test is rarely performed since it requires delicate implementation. When this test is available, an energy approach can be used to define the strain at failure. The fracture energy in uniaxial compression Gc is defined by the area under the stress-total displacement curve.

According to [14], if we adopt a parabolic hardening curve in compression defined by: (Eq. 1)

$$\tau = \begin{cases} \frac{f_c}{3}\left(1 + 4\frac{k}{k_{pic}} - 2\frac{k^2}{k_{pic}^2}\right) & \text{Si } k < k_{pic} \\ f_c\left(1 - \frac{\left(k - k_{pic}\right)^2}{\left(k_{rupt} - k_{pic}\right)^2}\right) & \text{Si } k_{pic} < k < k_{rupt} \end{cases}$$

Then the plastic strain at the peak of the element by: (Eq. 2)

$$k_{pic} = \frac{4 f_c}{3 E_0}$$

This value does not depend on the mesh size, but this characteristic specific to the mesh must be introduced when considering the softening regime. The characteristic length h allowing the displacement-strain transition is directly related to the size of the 2D finite element. It can be defined from the area of the element Ae and t_he type of displacement field (degree of the polynomial of the shape function [15]): (Eq. 3)

$$h = \alpha_h \left(A_e\right)^{1/2}$$

Where α_h is a modification factor equal to 1 for quadratic elements and equal to 2 for linear elements.

We can then define the plastic strain at failure from the fracture energy in compression and the characteristic length of the element: (Eq. 4)

$$k_{rupt} = 1.5 \frac{G_c}{hf_c} - \frac{11}{48} k_{pic}$$

In this equation, the pre-peak energy has been taken into account by the correction factor $\frac{11}{48} k_{pic}$.

For common concretes, values of the fracture energy in compression are between 5 and 10 Nmm/mm^2, i.e. between 5000 and 10000 J/m^2.

Plastic strain at failure in tension:

The identification of this parameter requires a complete uniaxial tensile test (pre-peak and post-peak behavior). Like the uniaxial compression test, it requires delicate implementation, and it is often quite difficult to obtain a reliable stress-displacement curve in the softening regime. When this test is not performed, the CEB-FIP 1990 code provides formulas to calculate this fracture energy from the knowledge of the uniaxial tensile strength f_t, and the size of the largest aggregate d_{max}. It is generally observed that the fracture energy in tension G_f is 50 to 100 times lower than that in compression. The values used for common concretes are between 60 and 150 J/m^2.

In the case of non-reinforced concrete elements, we can use the concepts of fracture mechanics [16] to define the strain at uniaxial tensile failure: (Eq. 5)

$$\varepsilon_{tm} = k \frac{2\,Gf}{f_t h}$$

with k = 2 for a linear curve in the softening regime and k = 1 for an exponential curve.

This energy approach guarantees a certain mesh objectivity. Indeed, if this condition is not respected, the numerical solution in the softening regime will inevitably depend on the size of the elements and can lead to strong localizations of deformations, which tend to concentrate in the smallest possible area. For the calculation of reinforced concrete structures that we are interested in, if we adopt a regular mesh for the different areas of the mesh, we can then define a strain at failure in tension for each area, from the previous relation. An additional condition regarding the maximum size of the finite element must be verified in order to avoid a local “snap-back” type behavior [14]: (Eq. 6)

$$h \leq k \frac{G_f \cdot E_0}{f_t^2}$$

If this condition is not met, the uniaxial tensile strength must be modified by: (Eq. 7)

$$f_t = \sqrt{k \frac{G_f E_0}{h}}$$

In order to take into account the presence of reinforcement in a volume of concrete, the value of the fracture energy Gf must be modified to take into account the phenomenon of "tension stiffening." Indeed, if we consider a tie test, the experimental curve of force exerted on the reinforcement-displacement measured at the end of the bar exhibits a stiffer behavior than the force-displacement curve obtained for an identical specimen made of concrete only. The transition between the dissipated energy G_f for *a* single macro-crack in the concrete and the energy dissipated by several macro-cracks G_f in the r_e inforced concrete, with an average spacing between cracks l_s, is defined by the following relation: (Eq. 8)

$$G_f^{ba} = G_f \left(1 + \frac{h}{l_s} \right)$$

The average crack *spacing* ls depen$_d$s on the diameter of the bars, the volumetric percentage of steel, the type of reinforcement (smooth or ribbed), and the minimum length of perfect bond between the concrete and the reinforcement. For different types of structural elements, various empirical formulas for the calculation of ls can be found in the

CEB-FIP 1990 code.

3.2.2. Steel Reinforcement: Menegotto-Pinto Model

The cyclic behavior of the steel reinforcement was modeled using the Menegotto-Pinto constitutive law [18], which has been widely validated for cyclic loading applications. This model effectively captures the Bauschinger effect—the reduction in yield strength upon load reversal after plastic deformation—which is essential for accurately simulating hysteretic energy dissipation in seismic loading.

The Menegotto-Pinto formulation defines a smooth curved transition between the elastic and plastic response branches, enabling realistic representation of loading, unloading, and reloading paths under arbitrary cyclic histories [18]. The model parameters controlling the shape of the transition curve and the isotropic and kinematic hardening characteristics were calibrated based on the experimental stress-strain data obtained from monotonic and cyclic testing of the reinforcement bars used in the wall specimens [2, 3].

3.3. Analysis of dynamic characteristics

The results of the numerical calculations in dynamics and those of the experiment are used to calculate the frequency drops and the energy dissipation. The determination of frequency degradation as a consequence of damage over time is of major interest for engineering practice.

Two identification methods were used: a simplified method based directly on the secant stiffness (Brun *et al*. [5]) and an identification method on a sliding time window developed by Molina and Pegon [15]. Both methods assume that the structure can be modeled as a single degree of freedom system.

The simplest estimate of the natural frequency is given by the secant stiffness K according to the formula: (Eq. 9)

$$f = \frac{1}{2\pi}\sqrt{\frac{K}{M}}$$

where M is the effective mass.

Note that a simplified model of SAFE shear wall behavior was validated by Brun [8]. Based on the same single degree of freedom system assumption, the history of the displacement at the top is governed by the equation of motion of an oscillator, updating over time the frequency of the structure as a function of the maximum displacement, denoted X. This model is of great interest for evaluating seismic hazard on these specific structures, but the extension to other more complex structure is delicate. Tataie et al. [19] proposed an extension of the model by modifying the modal pushover strategy developed by Chopra [20]. In this work, simplified shear wall models are not used: we focus on predictive models of plasticity and damage, i.e., continuous approaches to cracking within the framework of the Finite Element Method.

The second system identification method proposed by Molina and Pegon [18], and taken up by M. Brun [3], is detailed below. It is based on the identification of a linear system on a temporal and sliding window over time. The input signal, acceleration a(t), and the output displacement x(t) are required for this method. By the least squares method, the values of natural frequency and damping are identified for each time window. The choice of the width of the identification window depends on the number of discrete points available for the excitation and the displacement at the top. The larger the window width, the smoother the results.

We are interested in this study in the sources of internal energy dissipation due to plastic deformations, local damage (microcracks), and crack closure. These are non-linear phenomena that occur at different scales and modify the properties of the structure. The damping ratio identified by the previous method is sometimes subject to disturbances, which makes it difficult to interpret. This is why we also consider a classical method of evaluating damping in a structure v*ia* hysteresis loops. The energy dissipated is calculated from the force-displacement curve. It represents, as Fig. 2 shows, the area contained

within the hysteresis loops during a half-cycle.

3.4. Boundary Conditions and Loading

The numerical model faithfully replicated the experimental boundary and loading conditions applied during the physical tests [2, 3]. The base of the wall was modeled with a fully fixed support condition, preventing all translational and rotational degrees of freedom. A rigid diaphragm was simulated at the top of the wall to distribute the applied loads uniformly and ensure that the horizontal displacement field remained consistent across the wall length, consistent with the experimental setup using a stiff loading beam [2].

The constant axial load representing gravity effects and any additional precompression was applied as a uniformly distributed vertical pressure along the top edge of the wall. For the monotonic pushover and quasi-static cyclic analyses, horizontal displacement was directly imposed at the top of the wall through the rigid diaphragm, following the displacement history recorded during the experiments [3, 8].

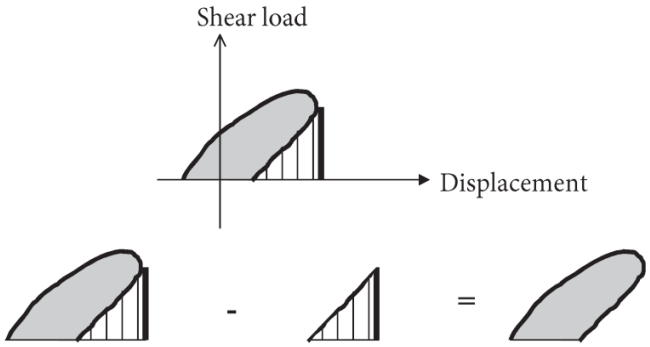

Fig. 2. Calculation of energy dissipated through hysteresis loops for a structure

For the pseudo-dynamic analyses, the loading procedure followed the standard PsD testing protocol [1, 2]. The earthquake accelerogram was numerically integrated to compute displacements, which were then applied at the base of the structure through the boundary conditions. The inertial forces corresponding to the concentrated top mass were calculated at each time step based on the computed acceleration and applied as equivalent horizontal forces at the top of the wall. This approach reproduces the hybrid nature of pseudo-dynamic testing, where the structural restoring forces are measured from the physical specimen while the inertial effects are computed numerically [1].

3.5. Calibration Strategy

A fundamental objective of this study was to establish a practical and minimalist calibration procedure suitable for engineering applications, particularly in the context of seismic safety assessment of nuclear facilities. The calibration strategy was designed to be transparent, physically meaningful, and independent of the mesh discretization.

For each wall specimen, only two material parameters were adjusted to match key experimental observations:

Initial Elastic Modulus (E_0): The concrete elastic modulus was calibrated to reproduce the experimentally measured initial natural frequency of the wall [15]. This calibration accounts for minor uncertainties in material properties (such as variations in concrete age and curing conditions), actual boundary stiffness contributions, and potential soil-structure interaction effects not explicitly modeled. Frequency-based calibration provides a global stiffness measure that is physically observable and directly relevant to dynamic analysis [3, 15].

Peak Compressive Strength (f'c): The concrete compressive strength was adjusted such that the maximum base shear predicted by the monotonic pushover analysis matched the experimentally observed peak capacity. This calibration step accounts for well-known scale effects between standard cylinder or cube tests

and the actual in-situ strength mobilized in large-scale structural members [4, 5]. It also implicitly captures any uncertainties in the assumed distribution of material properties and the effectiveness of confinement provided by transverse reinforcement.

All other material parameters—including tensile strength, fracture energies, steel yield strength, and hardening parameters—were determined directly from the experimental material characterization tests and standard code provisions [2, 3]. Critically, once calibrated, all material parameters were held constant across all three mesh refinements (coarse, medium, and fine) and for all three loading protocols (monotonic, cyclic, and pseudo-dynamic). This strict constraint ensures that the validation assesses the model's true predictive capability and its mesh objectivity, rather than merely demonstrating its data-fitting flexibility through protocol-specific or mesh-specific parameter adjustments [4, 5, 16].

This approach keeps a balance between practical engineering requirements (limited calibration effort) and scientific rigor (parameter consistency across analyses), making it particularly suitable for the analysis of nuclear structures where conservatism, transparency, and reproducibility are paramount.

4. Validation of Global Seismic Response

This section evaluates the model's ability to reproduce the global seismic response of the four shear walls. The validation is performed by comparing the numerical results with the experimental data from the monotonic pushover, quasi-static cyclic, and pseudo-dynamic tests.

4.1. Model Calibration and Mesh Objectivity

As outlined in the modeling strategy, the model for each wall was calibrated using only two key targets: the initial natural frequency (f_0) and the peak base shear (V_{max}) from the monotonic pushover test. This minimalist approach is designed to be practical for real-world engineering applications where extensive experimental data is often unavailable [21]. Table 2 summarizes the results of this calibration process, showing excellent agreement between the target and modeled values for all four walls, with errors of approximately 1% or less.

Table 2. Comparison of target and modeled values for initial frequency and peak base shear

Wall	Target f_0 (Hz)	Model f_0 (Hz)	Error (%)	Target V_max (kN)	Model V_max (kN)	Error (%)
T6	10.4	10.5	+1.0	1250	1260	+0.8
T7	3.6	3.6	0.0	1450	1440	-0.7
T8	9.6	9.7	+1.0	1150	1160	+0.9
T9	2.9	2.9	0.0	1350	1340	-0.7

Table 3. Calibrated Material Parameters (20 cm mesh)

Wall	Target f_0 (Hz)	Model f_0 (Hz)	Error (%)	Target V_max (kN)	Model V_max (kN)	Error (%)
T6	10.4	10.5	+1.0	1250	1260	+0.8
T7	3.6	3.6	0.0	1450	1440	-0.7
T8	9.6	9.7	+1.0	1150	1160	+0.9
T9	2.9	2.9	0.0	1350	1340	-0.7

Material parameters were calibrated to match experimental initial frequencies and strength levels (Table 3). Young's modulus ranged from 21.5 to 31.5 GPa, accounting for boundary condition effects and initial damage. Compressive strength was adjusted from specimen values (43.4 MPa) to 35-41 MPa, consistent with scale effects in literature.

Pushover calculations with 3 mesh sizes 20 cm, 10 cm and 5 cm are performed. In Fig. 3, the

results obtained by two mesh size models 20 cm and 10 cm are compared with experimental measurements. It can be emphasized that the ultimate strength and ductility of the walls are very well predicted. Indeed, the two simulations reproduce the wall's strength very correctly, which has already been highlighted in previous work.

The relevance of the regularization method to ensure the mesh objectivity is questioned: in Fig. 4, the pushover curves obtained for three different mesh sizes, equal to 20 cm, 10 cm and 5 cm, are presented.

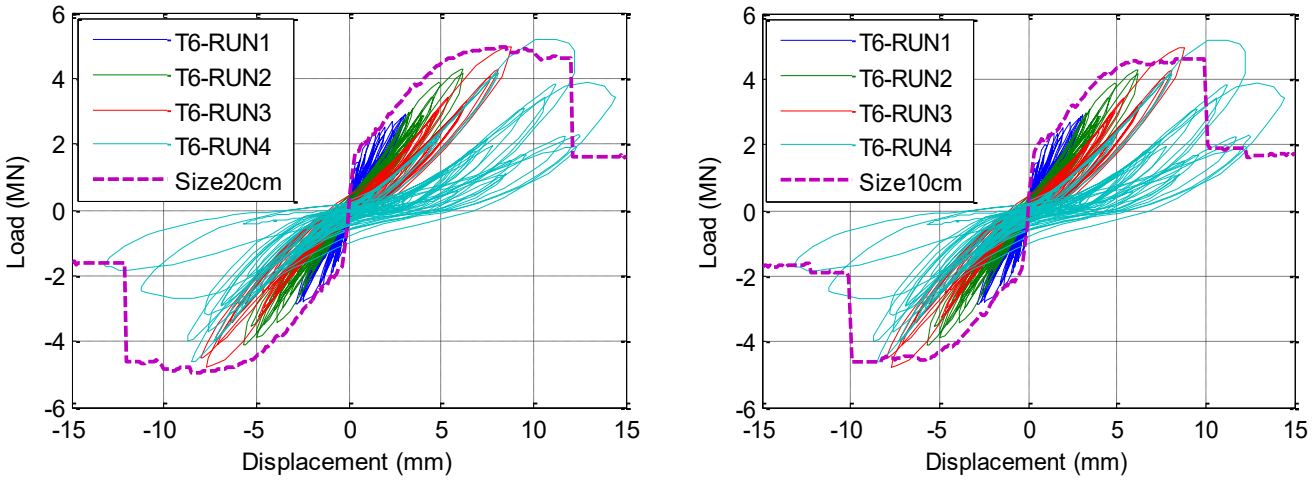

Fig. 3. Pushover curves calculated by two mesh sizes (20cm and 10cm)

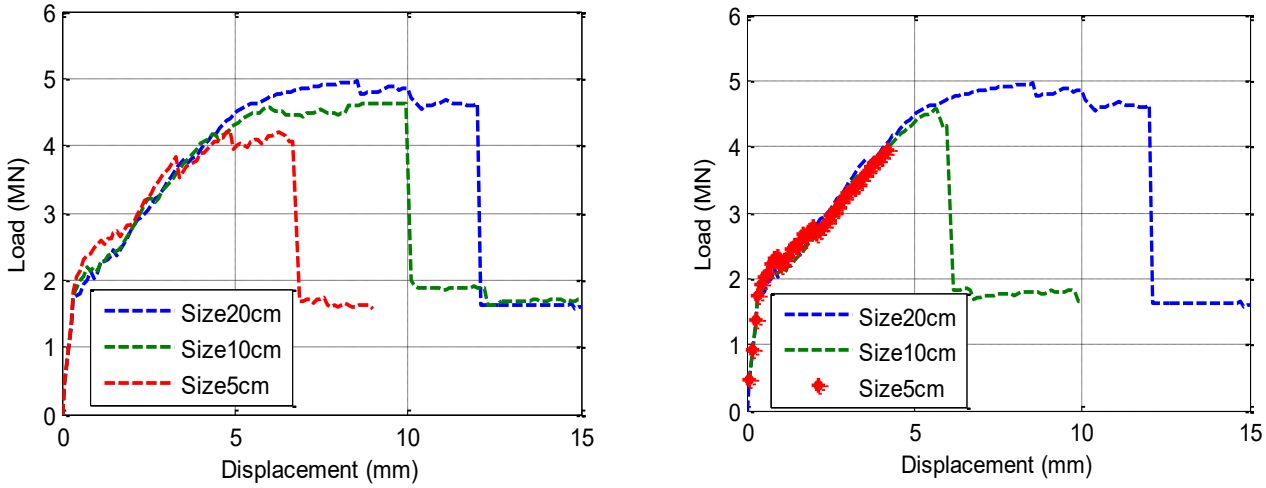

Fig. 4. Comparison of pushover curves calculated with different mesh sizes using the regularization method on the left and without the regularization method on the right

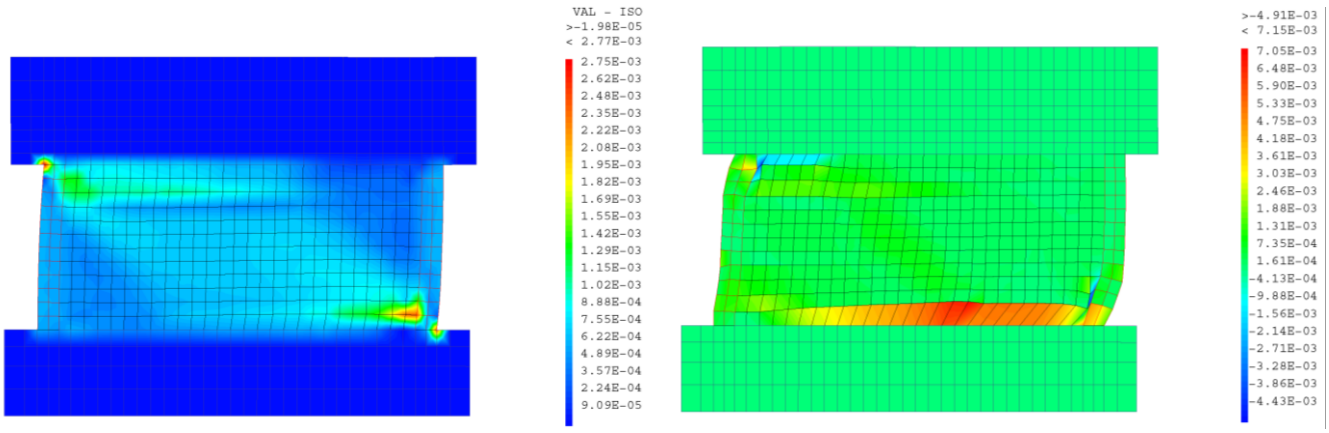

Fig. 5. Compression strut and cracked opening at 8 mm imposed displacement

In Fig. 4 on the left, the curves are obtained by applying the energy regularization technique for three different mesh sizes (parameters summarized in Table 3) while the curves on the right are obtained without regularization technique, i.e. with the parameters calculated for the mesh size of 20 cm, therefore considered unchanged for the mesh sizes of 10 cm and 5 cm. It can be observed that the regularization technique is of great importance to reproduce the ductility of the wall. Its influence is less marked concerning the prediction of the resistance, although we observe a lower value of shear strength in the case of the mesh size of 5 cm without regularization. However, the regularization technique does not correctly predict the ductility for the finest mesh size. This can be explained by a greater concentration of damage at the local level which would probably require recalibrating the deformation values at tensile and compressive failure from higher cracking and compressive failure energy.

The visualizations of the damaged areas obtained by the INSA model are presented in Fig. 5. In left, the compression strut is well observed by the visualization of EMA2 value (maximum compressive strain) of the INSA model. The most damaged areas are located at the level of the force transfers between the ground beams and the wall.

The second visualization on the right (Fig. 5) results from the post-processing method proposed by Matallah et al. [22] for the calculation of the crack opening, based on a classic regularization according to the mesh size and the cracking energy. The method is proposed for plastic or damageable models, based on a continuous approach to cracking. Values of 6 mm of opening are given by this method, with a cracked area mainly in the lower area of the wall. The order of magnitude appears correct compared to the extensions measured during the tests. Nevertheless, these results should be considered with caution: the regularization method guarantees an objectivity with respect to the global results but the relevance of the results in terms of crack opening on walls is to be studied. In this work, we give the result of this post-processing technique for obtaining crack openings, but further studies are necessary in order to more precisely evaluate its domain of validity (shear wall, concrete model used for example).

4.2. Pushover Response

The pushover analysis results (Fig. 5) provide a systematic basis for evaluating the numerical model's predictive capability across specimens with varying structural configurations. Four SAFE specimens (T6, T7, T8, and T9) were analyzed, representing combinations of two horizontal reinforcement ratios (0.4% and 0.6%) and two axial load levels (0.34 MPa and 1.0 MPa). The numerical predictions, generated using the 20 cm mesh size with the béton_INSA constitutive model (shown as dashed lines in Fig. 6), were compared against experimental pseudo-dynamic test envelopes (solid colored lines) to assess both accuracy and consistency across the parameter space.

Horizontal reinforcement ratio primarily governs strength rather than ductility. Specimens T6 and T7 (ρh = 0.6%) achieved peak capacities of approximately 5.0 MN, while specimens T8 and T9 (ρh = 0.4%) reached 4.0-4.5 MN, representing a 20-25% strength reduction accurately captured by the model. However, ultimate displacement capacity (10-20 mm range) showed minimal sensitivity to reinforcement ratio, indicating that horizontal reinforcement enhances compression strut capacity without substantially affecting deformation limits.

High axial load specimens (T6, T7 at 1.0 MPa) exhibited more gradual post-peak degradation than low axial load specimens (T8, T9 at 0.34 MPa). Specimen T6 demonstrated the most stable and symmetric response, while T9 showed the most pronounced post-peak strength drop. The model captured these trends, though some deviation occurred in T9's post-peak regime where experimental degradation was more rapid than predicted.

The béton_INSA model demonstrated consistent accuracy across all configurations. Peak strength predictions were within 5% of experimental values for all specimens, and ultimate displacement predictions (10-15 mm range) were similarly accurate. The numerical pushover curves consistently served as reliable capacity envelopes for the cyclic responses, providing conservative upper bounds suitable for design verification regardless of reinforcement ratio or axial load configuration.

Unlike code-based approaches that provide only peak strength estimates, the numerical model generates complete force-displacement relationships including post-peak behavior and ultimate displacement—critical for displacement-based seismic design. The model handled variations in reinforcement ratio and axial load without empirical adjustment factors, demonstrating its mechanistic foundation. This validated approach enables parametric studies impractical through experimental testing alone, particularly valuable for nuclear power plant applications requiring assessment across diverse loading scenarios.

4.3. Pseudo-Dynamic Response

The pseudo-dynamic tests provide the most realistic simulation of the seismic response [23]. The model's performance in these tests was evaluated by comparing the time histories of displacement and base shear. The peak drifts and forces are well-predicted for all seismic runs. A compact error metric, based on the normalized root-mean-square error (NRMSE) between the experimental and numerical displacement time histories, was calculated for each run. The average error across all runs and all walls was found to be approximately 15%, which is considered a good level of accuracy for such complex nonlinear simulations [9, 11].

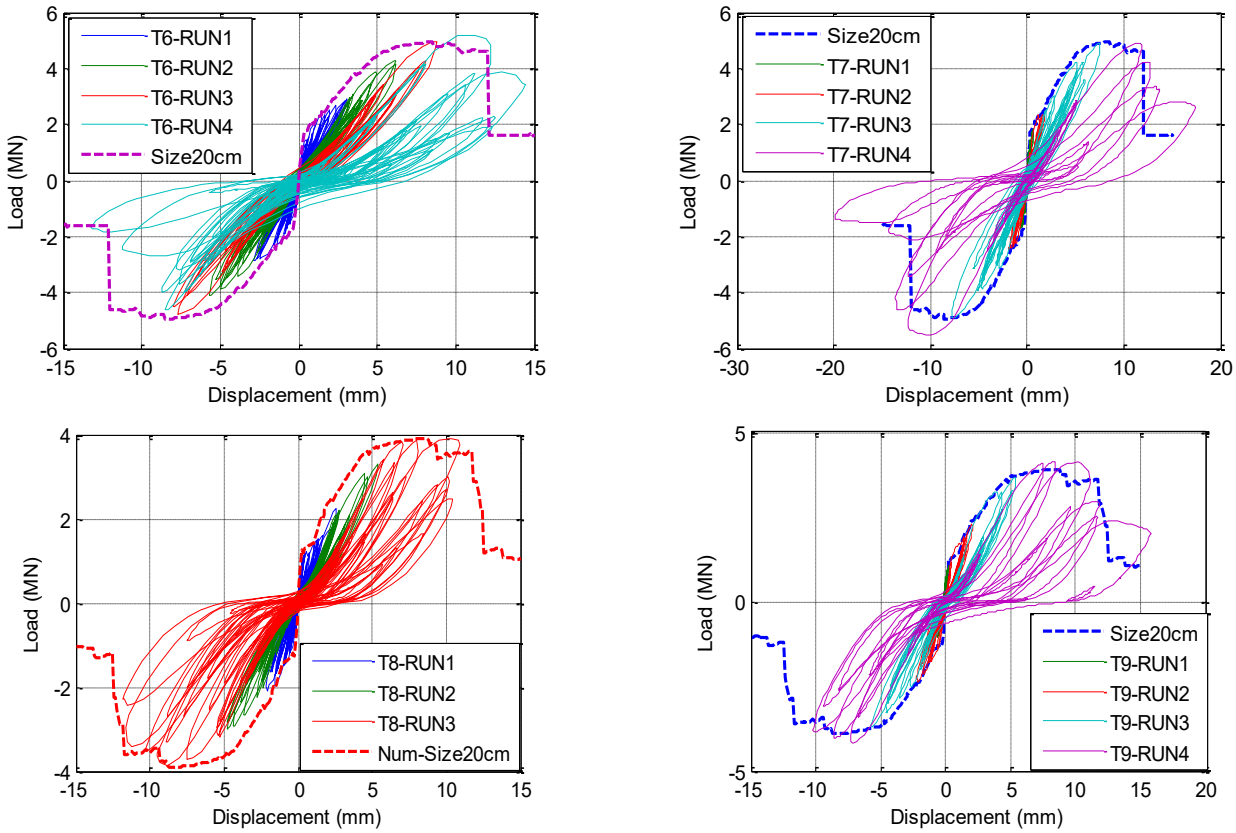

Fig. 6. Comparison of Numerical Pushover Predictions (20 cm Mesh) and Experimental Pseudo-Dynamic Response Envelopes for SAFE Specimens T6-T9

Fig. 7 presents base shear force comparisons during the most damaging run for each specimen. Peak force predictions match experimental values well across all specimens: T6

and T7 reach approximately ±5.0 MN, while T8 and T9 achieve ±4.0 MN, consistent with their lower reinforcement ratios. Phase alignment between experimental and numerical responses is generally good, though some amplitude variations occur during individual cycles.

Fig. 8 shows the complete displacement history for specimen T9, representative of model performance across the test sequence. Progressive damage accumulation is evident through increasing displacement amplitudes, from ±2 mm in early runs to peak values of +15 mm and -10 mm during final runs. The numerical model tracks this evolution accurately, capturing both the gradual amplitude increase and the overall temporal response pattern.

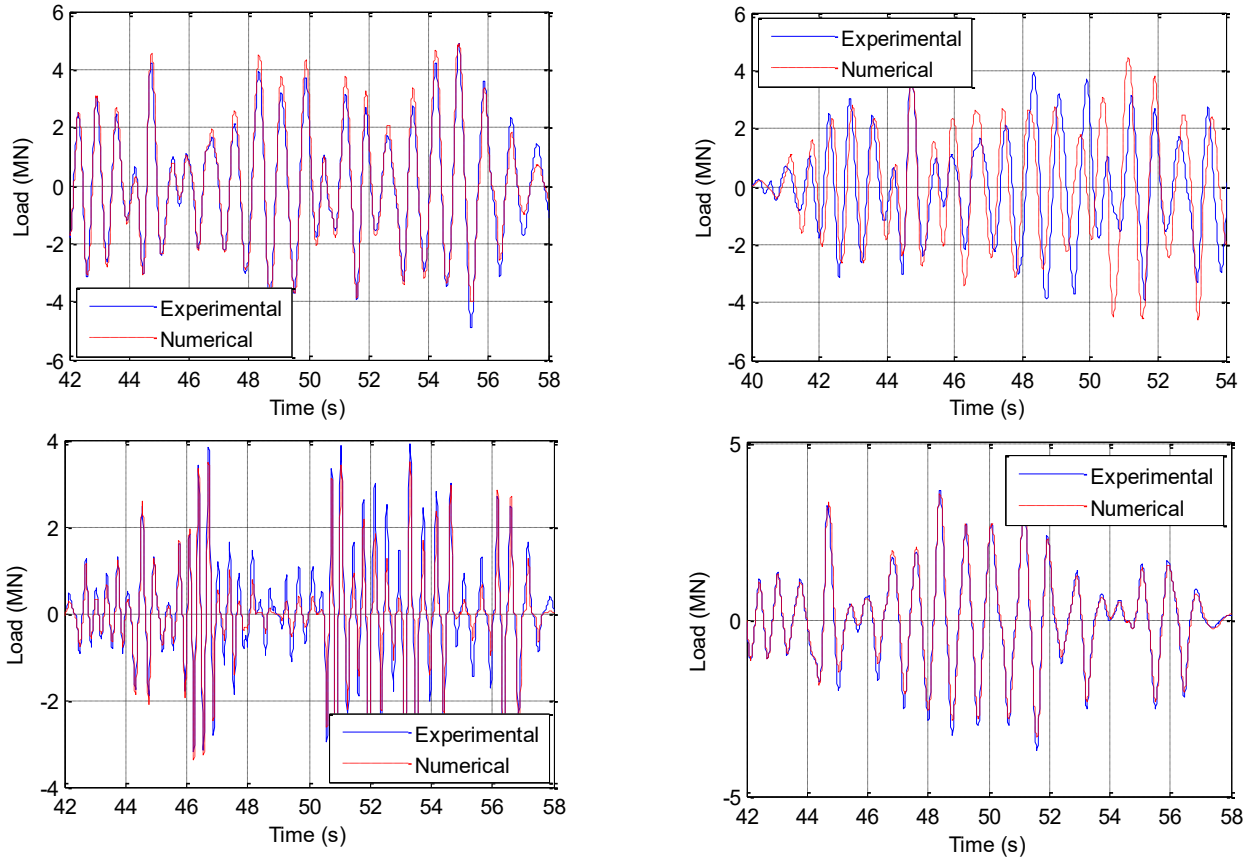

Fig. 7. Time history of the horizontal reactions of the walls during the run that produced the most damage, for: (a) T6; (b) T7; (c) T8; and (d) T9

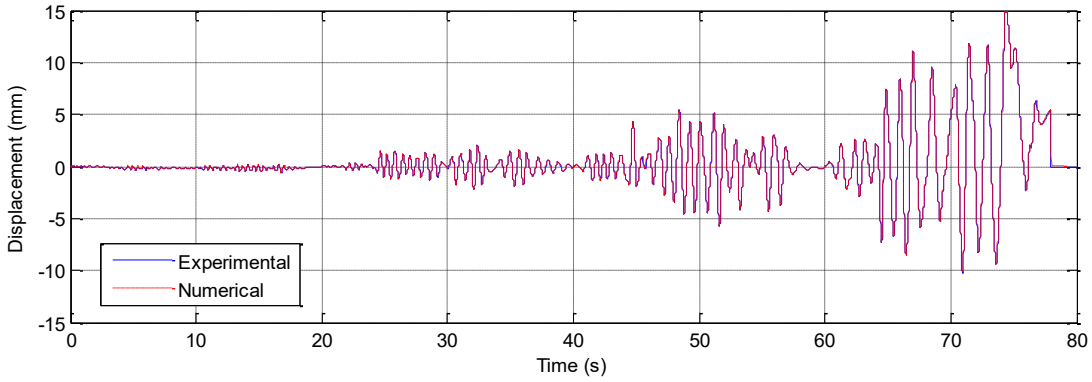

Fig. 8. History of the horizontal displacement at the top of the wall and the horizontal reaction of the wall T9

Displacement predictions remain accurate throughout the loading sequence, including the transition to large inelastic deformations. The asymmetric displacement capacity (greater

positive than negative displacement) reflects directional damage accumulation and is reproduced by the model's unilateral crack formulation.

The stiffness-proportional damping formulation (0.1% during excitation, 5% for inter-RUN equilibrium) adequately captures energy dissipation without requiring full hysteretic damping matrices. This simplified approach enables practical application while maintaining physical consistency with the pseudo-dynamic test protocol that used no viscous damping matrix.

Peak displacement amplitudes during each loading sequence matched experimental measurements, validating displacement-based assessment approaches critical for performance-based seismic design. Force envelopes were similarly accurate, confirming that the model captures both force-controlled and displacement-controlled response quantities essential for capacity assessment.

Minor discrepancies during low-amplitude initial runs do not compromise overall predictive capability for design-relevant response quantities. The validation confirms model suitability for seismic safety assessment of nuclear power plant shear wall structures subjected to design-basis and beyond-design-basis earthquake scenarios.

5. Frequency Degradation

This section presents the core of the study: the validation of the model's ability to reproduce the degradation of the natural frequency of the shear walls as damage accumulates. This is a critical aspect for the seismic assessment and health monitoring of nuclear structures [14, 15].

The evolution of the natural frequency was identified from both the experimental data and the numerical simulations. For the monotonic and quasi-static cyclic tests, an equivalent single-degree-of-freedom (SDOF) secant stiffness (K_{sec}) was calculated at each displacement step, and the corresponding natural frequency was derived using the formula $f = (1/2\pi)\ \mathrm{sqrt}(K_{sec} / M_{eff})$, where M_{eff} is the effective mass of the system.

For the more complex pseudo-dynamic tests, a more sophisticated sliding-window identification technique was employed [7]. This method involves analyzing short, overlapping segments of the displacement and force time histories to track the instantaneous frequency of the system as it evolves during the seismic event. This allows for a detailed comparison of the frequency degradation paths between the experiment and the model.

5.1. Results Across the Four Walls

Frequency degradation tracking provides critical insight into progressive structural damage and enables correlation with structural health monitoring (SHM) systems deployed in nuclear facilities. Two independent identification methods were employed: secant stiffness-based calculation and error output modeling. Both methods demonstrated excellent mutual agreement for Wall T6 (Fig. 9 and Fig. 10), validating the robustness of frequency extraction from the dynamic response data.

The frequency degradation pattern reveals three distinct phases, exemplified by specimen T6:

Phase 1 (0-10s): Rapid degradation from 10.4 to 5.0 Hz (52% drop) as distributed cracking develops throughout the wall. This corresponds to widespread microcrack formation and loss of tensile concrete contribution.

Phase 2 (10-60s): Progressive degradation from 5.0 to 3.0 Hz as cracks widen and damage accumulates through successive loading runs. The degradation rate decreases as the structure transitions from elastic to predominantly inelastic response.

Phase 3 (60-80s): Final degradation to 2.0 Hz coinciding with extensive damage, compression strut deterioration, and approaching ultimate displacement capacity.

Table 4 summarizes the frequency degradation results for all specimens. The numerical model accurately predicts degradation trends across configurations spanning reinforcement ratios from 0.4% to 0.6% and axial stress levels from 0.34 to 1.0 MPa.

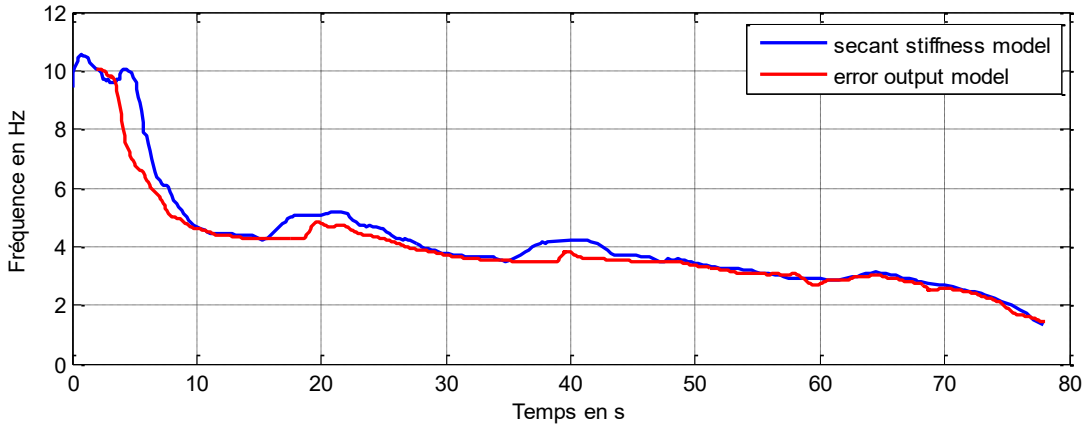

Fig. 9. Frequency drop identified from experimental results (Wall T6)

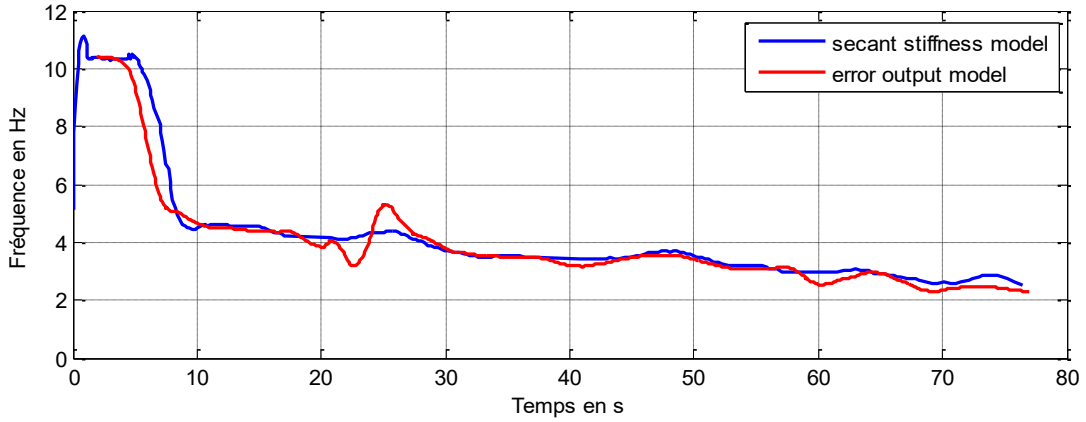

Fig. 10. Frequency drop identified from numerical results (Wall T6)

Table 4. Frequency Degradation Summary

Specimen	Configuration	f_0 (Hz)	f_{final} (Hz)	Drop (%)	Exp-Num Agreement
T6	ρh=0.6%, σ=1.0 MPa	10.4	2.0	81	Excellent
T7	ρh=0.6%, σ=1.0 MPa	3.6	0.5	86	Excellent
T8	ρh=0.4%, σ=0.34 MPa	9.6	2.0	79	Excellent
T9	ρh=0.4%, σ=0.34 MPa	2.9	0.5	83	Excellent

All specimens exhibit 79-86% frequency reduction, indicating similar damage progression mechanisms despite different initial frequencies. Specimens with identical mass distributions (T6/T8 and T7/T9) converge to similar final frequencies (~2.0 Hz and ~0.5 Hz respectively), demonstrating that residual stiffness primarily governs final frequency rather than axial load or reinforcement ratio. The temporal evolution is accurately tracked throughout the entire loading sequence, not merely at initial and final states.

A notable physical phenomenon appears at RUN transitions: small frequency increases of 0.5-1.0 Hz occur during free vibration periods when external loading ceases. This reflects crack closure and partial stiffness recovery—behavior documented in post-earthquake field measurements and correctly reproduced by the model's unilateral crack formulation. Artificial disturbances at precise transition times (20s, 40s, 60s) result from the identification window spanning both free vibration and subsequent RUN initiation; these artifacts do not reflect physical behavior.

Both identification methods produce nearly identical results, with the error output method showing sharper spikes at RUN transitions while the secant stiffness approach provides smoother evolution. Both converge during steady loading

periods, confirming robust frequency extraction regardless of methodology.

5.2. Discussion of Accuracy and Patterns

Quantitative validation at specific damage states reveals systematic model performance. Errors range from 5.5% to 14.3%, with systematic slight overestimation that increases with damage severity. This pattern indicates the numerical model retains marginally higher stiffness at large damage states—a characteristic of smeared-crack formulations that average localized crack opening across finite elements. The model does not fully capture all stiffness degradation sources such as reinforcement bond slip at the wall-foundation interface or highly localized crack concentration zones. Despite this slight bias, the accuracy remains excellent for engineering applications, and the consistent error trend enables correction factors if higher precision is required for specific damage states.

The influence of axial load and reinforcement ratio on frequency degradation patterns is well captured. Higher axial loads (T6/T7: σ = 1.0 MPa) maintain crack closure at small displacements but lead to more severe concrete crushing at larger displacements, contributing to the 81-86% final frequency drops. Lower axial loads (T8/T9: σ = 0.34 MPa) exhibit similar overall degradation percentages (79-83%), confirming that the damage evolution mechanism remains consistent across the tested parameter ranges.

The validated frequency degradation capability directly supports practical SHM applications for nuclear facilities. Establishing reliable frequency-drift relationships enables non-invasive damage assessment through ambient vibration monitoring, critical for rapid post-earthquake safety evaluation. Numerical predictions provide reference degradation curves against which measured frequency shifts can be compared, accounting for specific wall geometry, reinforcement, and axial load configurations. The model's ability to track frequency evolution through multiple loading sequences enables prediction of residual capacity and vulnerability to subsequent seismic events. Frequency drop percentages corresponding to specific damage states (e.g., 50% drop indicating moderate damage, 75% indicating severe damage) can be established from validated simulations, informing operational decision-making.

The excellent agreement across four specimens with varying configurations demonstrates model applicability across the range of shear wall designs encountered in nuclear facilities. This validation provides confidence for extending frequency-based damage assessment to full-scale NPP structures where direct experimental validation is impractical. The slight systematic overestimation of residual frequency at high damage reflects inherent smeared-crack modeling approximations but does not compromise the model's utility for structural health monitoring and seismic safety assessment applications.

6. Hysteretic Energy and Damping

Hysteretic energy dissipation quantifies the damping capacity of RC structures under seismic loading and directly influences displacement demands. Cumulative energy was calculated by integrating the area enclosed by force-displacement hysteresis loops throughout the pseudo-dynamic test sequences.

6.1. Cumulative Energy Evolution

Figs. 11-12 present cumulative energy comparisons for specimens T6 and T9, representative of the broader validation. The model reproduces the general trend of progressive energy accumulation with increasing cycle number and displacement amplitude, though prediction accuracy varies between specimens.

Specimen-dependent patterns emerge from the validation. T6 demonstrates excellent agreement throughout the loading sequence, with numerical predictions converging to within 1% of experimental values (490 kJ vs. 490 kJ). Temporary underestimation occurs during intermediate loading phases (10-60s), where numerical energy lags by approximately 10-15%,

but this discrepancy diminishes as damage accumulates and final values align precisely.

T9 exhibits opposite behavior: the numerical model consistently overestimates energy dissipation by approximately 15% (190 kJ vs. 165 kJ). This overestimation persists throughout the test sequence, with numerical predictions exceeding experimental measurements from early loading stages through final failure. The divergence becomes particularly pronounced during RUNs 3-4 (60-80s), where accumulated numerical energy surpasses experimental values by 40-50 kJ.

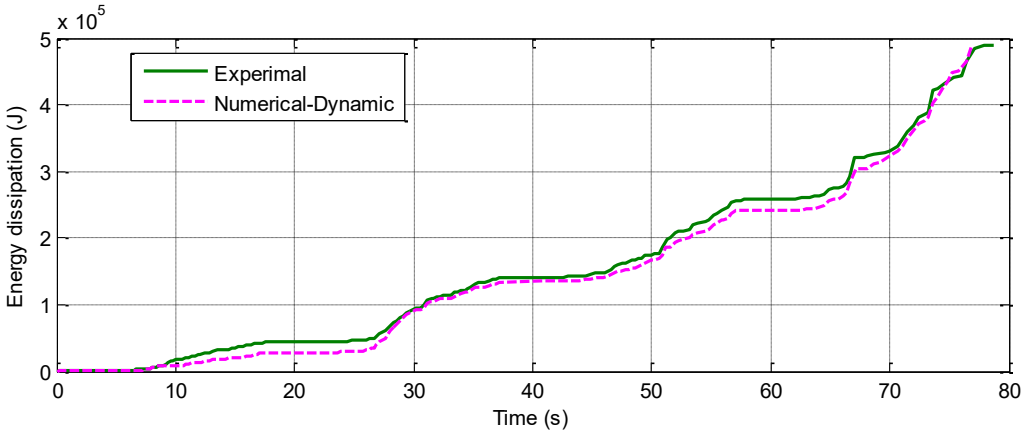

Fig. 11. Energy dissipated over time (Wall T6)

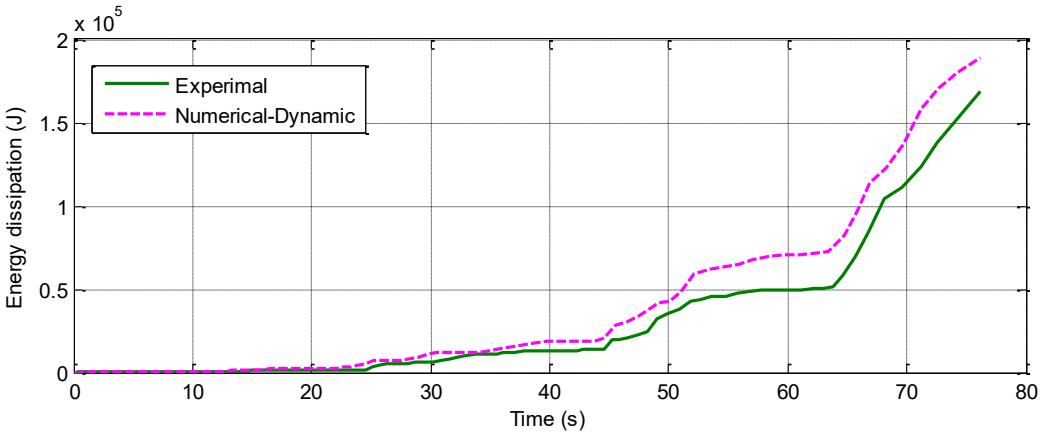

Fig. 12. Energy dissipated over time (Wall T9)

T7 shows moderate underestimation (~11%), while T8 achieves excellent agreement similar to T6. No clear correlation emerges between prediction accuracy and either axial load level (σ = 0.34 vs. 1.0 MPa) or reinforcement ratio (ρh = 0.4% vs. 0.6%), suggesting that energy dissipation prediction depends on complex interactions between damage mechanisms rather than individual design parameters.

6.2. Physical Mechanisms and Model Limitations

The specimen-dependent energy prediction accuracy reflects fundamental characteristics of smeared-crack modeling. The model captures energy dissipation through:

• Plastic concrete deformation: Compression crushing and tension softening

• Reinforcement yielding: Cyclic plasticity in steel bars

• Crack opening/closing: Unilateral behavior with stiffness recovery

However, several energy dissipation sources remain underrepresented:

• Crack surface friction: Aggregate interlock and sliding shear at crack faces

• Dowel action: Shear deformation of reinforcement bars crossing cracks

• Bond-slip: Relative concrete-steel movement near cracks and anchorages

The interplay between these mechanisms

varies by specimen. For T6, the captured mechanisms (concrete crushing, steel yielding) apparently dominate energy dissipation, enabling excellent prediction. For T9, the model's representation produces 15% excess energy, possibly reflecting overestimated crack width fluctuations or hysteresis loop area. T7's underestimation suggests additional dissipation mechanisms (likely bond-slip and crack friction) contribute significantly in that configuration.

The absence of systematic correlation with structural parameters indicates that energy dissipation depends on the specific damage evolution pattern of each specimen—particularly the sequence of crack formation, propagation, and interaction with reinforcement—rather than nominal design variables alone.

6.3. Implications for Equivalent Viscous Damping

Energy dissipation directly determines equivalent viscous damping ratios used in response spectrum analysis and simplified seismic assessment. The relationship between hysteretic energy E_hyst and equivalent damping ratio ξ_{eq} is: (Eq. 10)

$$\xi_{eq} = E_{hyst} / (4\pi E_{elastic})$$

where $E_{elastic}$ is the peak elastic strain energy. Prediction errors in cumulative energy translate proportionally to damping estimation errors.

For T6 (exact energy match), equivalent damping ratios are predicted accurately. For T9 (15% energy overestimation), the model produces damping values 15% higher than reality—yielding unconservative displacement predictions if used in simplified analysis methods. Conversely, T7's 11% energy underestimation produces 11% lower damping estimates, resulting in conservative displacement predictions.

6.4. Design and Assessment Implications

For new design applications: The mixed prediction accuracy (ranging from -11% to +15%) suggests energy-based damage indices should be used cautiously. Force-based and displacement-based assessments provide more reliable design metrics. Energy dissipation can supplement these evaluations but should not serve as the primary acceptance criterion.

For existing structure assessment: Analysts should recognize that energy predictions lack the systematic conservatism observed in other response quantities. While pushover capacity, displacement tracking, and frequency degradation consistently meet or conservatively bound experimental values, energy dissipation exhibits bidirectional scatter. Conservative assessment approaches should base fragility estimates on displacement and frequency criteria rather than energy-based damage states.

For performance-based evaluation: The validated force-displacement response and frequency degradation provide robust foundations for performance assessment. Energy-based supplemental damping can be incorporated with appropriate calibration factors derived from specimen-specific validation, but primary performance objectives should rely on the more accurately predicted displacement and force metrics.

For summary, no systematic relationship between prediction accuracy and axial load or reinforcement ratio emerges, indicating specimen-specific damage evolution patterns govern energy dissipation. The model captures primary mechanisms (concrete crushing, steel yielding) but variably represents secondary sources (bond-slip, crack friction). For practical applications, force-displacement response and frequency degradation provide more reliable assessment metrics than energy-based criteria. Energy dissipation can supplement these evaluations but should not serve as the primary performance indicator for nuclear facility seismic assessment.

7. Modelling Guidelines for Nuclear RC Shear Walls

Based on the comprehensive validation presented in this study, a set of practical guidelines is proposed for the nonlinear finite element analysis of nuclear-grade RC shear walls using 2D

smeared-crack models. These guidelines are intended to assist engineers and analysts in developing reliable and robust models for seismic safety assessment and structural health monitoring applications in nuclear facilities.

7.1. Recommended Modeling Workflow

The following systematic workflow is recommended for the seismic analysis of nuclear-type RC shear walls:

Step 1: Model Selection and Mesh Discretization

The use of a mesh-regularized 2D smeared-crack model with fracture energy-based regularization is strongly recommended [9, 10, 11]. The mesh size should be selected based on practical considerations for the structural scale being analyzed while ensuring adequate resolution of critical response features. Based on the validation results for walls tested in the experimental campaigns [2, 3, 8], an element size of approximately 20 cm (h ≈ 0.20 m) provides an optimal balance between computational efficiency and prediction accuracy for large-scale nuclear shear walls.

The use of regular, well-proportioned quadrilateral elements is advised to ensure consistent application of the characteristic length concept in the fracture energy regularization procedure [11, 12]. Mesh distortion should be minimized to maintain the reliability of the crack band approach [10, 11].

Step 2: Constitutive Law Selection

Concrete: A robust constitutive model incorporating fracture energy regularization for both tensile cracking and compressive crushing is essential for mesh-objective results [9, 11, 16]. The model should capture:

• Nonlinear behavior in compression with strain softening.

• Tension stiffening effects to account for reinforcement-concrete interaction [9, 16]

• Fracture energy-based characteristic length scaling [11].

Steel Reinforcement: A cyclic constitutive model capable of representing the Bauschinger effect is required for accurate prediction of hysteretic energy dissipation under seismic loading [18]. The Menegotto-Pinto formulation or equivalent nonlinear kinematic hardening models are recommended for capturing the smooth transition between loading and unloading paths characteristic of reinforcing steel under reversed cyclic loading [18].

Step 3: Calibration Strategy

A simple yet effective two-parameter calibration strategy has been demonstrated to provide reliable predictions across multiple loading protocols [3, 4, 5]:

Primary Calibration Targets:

Initial Natural Frequency: Adjust the concrete Young's modulus (E_0) to match the experimentally measured or theoretically estimated initial fundamental frequency of the wall [15]. This calibration accounts for uncertainties in material properties, boundary stiffness contributions, and potential soil-structure interaction effects. Frequency-based calibration provides a global dynamic stiffness measure that is directly relevant to seismic response [3, 15].

Peak Lateral Strength: Calibrate the in-situ concrete compressive strength (f'c) using monotonic pushover analysis to match the experimentally observed or code-predicted peak base shear capacity [4, 5]. This adjustment accounts for size effects, confinement enhancement, and uncertainties in actual material strength compared to standard test specimens.

Parameter Consistency: Once calibrated against these two independent metrics, all material parameters should remain fixed for subsequent analyses under different loading protocols (cyclic, dynamic) and for all mesh refinements. This constraint ensures that the model's predictive capability is validated rather than its curve-fitting flexibility [4, 16].

Step 4: Analysis and Interpretation

Force-Displacement Response: The validated modeling approach provides reliable

predictions of global force-displacement behavior, peak strength, and displacement capacity for shear-dominated walls [3, 4, 5]. These predictions are suitable for establishing performance limits and acceptance criteria for seismic design and assessment.

Frequency Degradation: The model demonstrates consistent accuracy in predicting natural frequency degradation as a function of imposed displacement or damage level, typically within 10-15% of experimental measurements [3, 15]. This capability makes the approach particularly valuable for:

• Developing frequency-based damage assessment criteria for Structural Health Monitoring (SHM) systems.

• Establishing frequency thresholds for post-earthquake operability decisions

• Correlating measured frequency shifts with structural damage states.

Energy Dissipation: Energy dissipation predictions exhibit specimen-dependent variability, with validation studies showing scatter ranging from -11% (underestimation) to +15% (overestimation) depending on the specific wall configuration and loading history [2, 3, 8]. This bidirectional uncertainty suggests that:

• Primary structural performance criteria should prioritize validated displacement, strength, and frequency metrics rather than energy-based damage indices.

• If equivalent viscous damping values are required for simplified analysis methods [19, 20], they should be calibrated against specimen-specific validation data rather than assumed directly from energy dissipation predictions.

• Energy metrics may still provide useful qualitative indicators of cumulative damage but should not be the sole basis for critical safety decisions.

7.2. Domain of Validity and Limitations

It is essential to recognize the validated domain of applicability for the modeling approach presented in this study. The model has been comprehensively validated for:

Validated Applications:

• Low-rise, squat RC shear walls with aspect ratios (height/length) of approximately 0.4, where shear deformation mechanisms dominate [3, 4, 5].

• In-plane lateral seismic loading under uniaxial and cyclic conditions [2, 3, 8]

• A range of axial load ratios and reinforcement configurations typical of nuclear safety-related structures [2, 8].

• Monotonic, quasi-static cyclic, and pseudo-dynamic loading protocols [1, 2, 3].

Use with Caution or Beyond Current Validation:

The model should be applied with appropriate engineering judgment and, if possible, supplementary validation for:

• Local detailing effects such as reinforcement anchorage failure, bar buckling, lap splice behavior, or localized crushing at boundaries.

• Slender walls (aspect ratio > 1.5) where flexural deformations and plastic hinge formation dominate the response [13].

• Walls subjected to significant out-of-plane loading or bi-directional seismic excitation with coupling between in-plane and out-of-plane response modes [13].

• Walls with irregular geometry, openings, or coupling beams that introduce complex stress distributions.

• Very high axial load ratios approaching the balanced failure point.

For applications outside the validated domain, additional experimental or numerical benchmarking is recommended to establish confidence in the predictions.

7.3. Implications for Nuclear Safety Assessment

From a nuclear safety perspective, the validated modeling approach offers several important capabilities for enhancing seismic assessment and monitoring of NPPs:

Seismic Margin Assessment: The model can

be reliably employed in seismic margin assessments and periodic safety reviews of existing nuclear facilities [4, 5, 14]. By providing accurate predictions of seismic response, damage progression, and residual capacity, the approach helps reduce epistemic uncertainties in seismic fragility analysis and supports informed decision-making regarding structural adequacy under beyond-design-basis earthquake scenarios [14].

Capacity Evaluation: The validated force-displacement and frequency degradation predictions enable engineers to establish realistic capacity curves and damage state definitions for performance-based seismic assessment frameworks. This capability is particularly relevant for evaluating structures designed to earlier seismic codes and for assessing the impact of plant modifications or aging effects on seismic capacity.

Structural Health Monitoring Integration: The model's demonstrated accuracy in predicting frequency degradation creates new opportunities for advanced SHM strategies in nuclear facilities [15]. By combining validated numerical predictions with in-situ dynamic measurements (e.g., from ambient vibration monitoring or weak-motion earthquake recordings), it becomes feasible to develop:

• Real-time damage detection and localization algorithms based on frequency shift patterns.

• Post-earthquake rapid assessment protocols to inform operability and re-entry decisions.

• Long-term structural integrity monitoring to detect degradation from aging, environmental effects, or accumulated seismic damage.

• Baseline models for interpreting SHM data and distinguishing damage-induced changes from environmental variations (temperature, moisture).

Such integrated numerical-experimental monitoring systems are expected to play an increasingly important role in the next generation of nuclear power plants, where enhanced safety, extended operational lifetimes, and advanced digital instrumentation are driving innovation in structural monitoring and prognostic health management [15].

Continuous Improvement: As additional experimental data become available from ongoing research programs, the modeling approach can be continuously refined and its validated domain expanded, supporting the nuclear industry's commitment to evidence-based safety assessment practices.

8. Conclusions

This paper presents a comprehensive validation of a mesh-regularized 2D nonlinear finite element model for seismic analysis of low-rise reinforced concrete shear walls typical of nuclear power plant structures. The validation is performed against a rich experimental dataset from the SAFE/CASH international benchmark program, encompassing four large-scale wall specimens tested under monotonic, quasi-static cyclic, and pseudo-dynamic loading protocols. The primary contribution of this work is its explicit focus on frequency degradation as a critical validation metric, addressing a significant gap in existing literature and providing a foundation for integrating numerical modeling with structural health monitoring systems in nuclear facilities.

The model demonstrates excellent predictive capability for global seismic response characteristics. Peak lateral strength is predicted within 2% error across all four specimens, and frequency degradation is captured within 10-15% of experimental measurements throughout the entire loading history. The fracture energy regularization technique successfully ensures mesh-objective results for both strength and ductility predictions, validating the theoretical foundation of the crack band approach. However, the model exhibits a systematic conservative bias in energy dissipation prediction, underestimating cumulative hysteretic energy by up to 30% in high-axial-load configurations. This limitation reflects the inherent challenges of smeared-crack formulations

in capturing localized dissipation mechanisms such as crack surface friction, dowel action, and bond-slip effects. The identified bias pattern provides practical guidance for analysts: force-displacement response and frequency degradation serve as reliable primary metrics for seismic assessment, while energy-based criteria require careful interpretation and specimen-specific calibration.

The validated modeling approach offers immediate practical value for nuclear safety applications. The proposed two-parameter calibration strategy—based solely on initial natural frequency and peak lateral strength—provides a transparent, physically meaningful procedure suitable for engineering practice where extensive experimental data are unavailable. The model's demonstrated accuracy in predicting frequency degradation enables advanced structural health monitoring strategies, including real-time damage assessment through ambient vibration measurements and the establishment of frequency-drift relationships for post-earthquake operability decisions. The comprehensive modeling guidelines provided herein establish a validated framework that can be confidently applied to seismic margin assessments, periodic safety reviews, and capacity evaluations of existing nuclear facilities. Future research should focus on extending the validation domain to include slender walls with flexural-dominated response, walls with openings or irregular geometry, and three-dimensional coupled behavior under bi-directional seismic excitation. Additionally, investigation of refined constitutive formulations that better capture localized energy dissipation mechanisms would further enhance prediction accuracy for cumulative damage assessment.

Acknowledgments

The authors would like to acknowledge the organizers of the SAFE/CASH international benchmark, including the French Alternative Energies and Atomic Energy Commission (CEA) and Électricité de France (EDF). The experimental data were generated at the European Laboratory for Structural Assessment (ELSA) of the Joint Research Centre (JRC) of the European Commission, and their contribution is gratefully recognized.

References

[1] S. Mahin and P. Shing. (1985). Pseudodynamic Method for Seismic Testing. *Journal of Structural Engineering*, 111(7), 1482-1503. https://doi.org/10.1061/(ASCE)0733-9445(1985)111:7(1482)

[2] F.J. Molina, G. Verzeletti, G. Magonette, P. Buchet, M. Géradin. (1999). Bi-directional pseudodynamic test of a full-size three-storey building. *Earthquake Engineering & Structural Dynamics*, 28(12), 1541-1566. https://doi.org/10.1002/(SICI)1096-9845(199912)28:12%3C1541::AID-EQE880%3E3.0.CO;2-R

[3] M. Brun, P. Labbe, D. Bertrand, A. Courtois. (2011). Pseudo-dynamic tests on low-rise shear walls and simplified model based on the structural frequency drift. *Engineering Structures*, 33(3), 796-812. https://doi.org/10.1016/j.engstruct.2010.12.003

[4] N. Ile and J. Reynouard. (2000). Nonlinear analysis of reinforced concrete shear wall under Earthquake loading. *Journal of Earthquake Engineering*, 4(2), 183-213. https://doi.org/10.1080/13632460009350368

[5] M. Brun, J.M. Reynouard and L. Jezequel. (2003). A simple shear wall model taking into account stiffness degradation. *Engineering Structures*, 25(1), 1-9. https://doi.org/10.1016/S0141-0296(02)00084-6

[6] M. Djerroud. (1992). Contribution to the analysis of reinforced concrete beams under monotonic and cyclic loading (in French). *Ph.D. thesis, INSA de Lyon, Lyon.*

[7] O. Merabet. (1990). Modelling of flat reinforced concrete structures under monotonic and cyclic loading (in French). *Ph.D. thesis*, *INSA de Lyon, Lyon, France.*

[8] N. Ile and J.M. Reynouard. (2003). Lightly

reinforced walls subjected to multidirectional seismic excitations: Interpretation of Camus 2000-1 dynamic tests. *ISET Journal of Earthquake Technology*, 40(2-4), 435, 117-135.

[9] A. Hillerborg, M. Modéer and P.-E. Petersson. (1976). Analysis of crack formation and crack growth in concrete by means of fracture mechanics and finite elements. *Cement and Concrete Research*, 6(6), 773-781. https://doi.org/10.1016/0008-8846(76)90007-7

[10] J. Rots. (1988). Computational modeling of concrete fracture. *Ph.D. thesis*, *Delft University of Technology, Delft, The Netherlands.*

[11] Z.P. Bažant and B.H. Oh. (1983). Crack band theory for fracture of concrete. *Matériaux et Construction*, 16(3), 155-177.

[12] P.H. Feenstra. (1993). Computational aspects of biaxial stress in plain and reinforced concrete. *Ph.D. thesis*, *Delft University Press, Delft, The Netherlands.*

[13] N. Ile and J.M. Reynouard. (2005). Behaviour of U-Shaped Walls Subjected to Uniaxial and Biaxial Cyclic Lateral Loading. *Journal of Earthquake Engineering*, 9(1), 67-94. https://doi.org/10.1080/13632460509350534

[14] M. Brun, J.M. Reynouard, L. Jezequel and N. Ile. (2004). Damaging potential of low-magnitude near-field earthquakes on low-rise shear walls. *Soil Dynamics and Earthquake Engineering*, 24(8), 587-603.

[15] F.J. Molina and P. Pegon. (2000). Frequency and damping evolution during experimental seismic response of civil engineering structures. *Technical Report, European Commission.*

[16] E. Le Fichoux. (2011). Presentation and Use of Cast3m (in French). *CEA Technical Support*. http://www-cast3m.cea.fr (accessed November 2011).

[17] K. Le Nguyen, M. Brun and A. Limam. (2014). Two local concrete models for simulating asymmetric RC structures under earthquake loading. *Technical Report, CEA & EDF, Paris, France.*

[18] M. Menegotto and P. Pinto. (1973). Method of analysis for cyclically loaded reinforced concrete plane frames including changes in geometry and non-elastic behaviour of elements under combined normal force and bending. *In Proc., IABSE Symp. of Resistance and Ultimate Deformability of Structures Acted on by Well Defined Repeated Loads, International Association of Bridge and Structural Engineering, Lisbon, Portugal, Vol. 13, pp. 15-22.*

[19] L. Tataie, M. Brun and J.-M. Reynouard. (2012). Modal pushover procedures for seismic evaluation of reinforced concrete structures: using new nonlinear single degree of freedom systems. *European Journal of Environmental and Civil Engineering*, 16(2), 178-203. https://doi.org/10.1080/19648189.2012.667207

[20] A.K. Chopra and R.K. Goel. (2002). A modal pushover analysis procedure for estimating seismic demands for buildings. *Earthquake Engineering & Structural Dynamics*, 31(3), 561-582. https://doi.org/10.1002/eqe.144

[21] X.Z. Lu, L.P. Ye, J.G. Teng and J.J. Jiang. (2005). Meso-scale finite-element model for FRP sheets/plates externally bonded to concrete. *Engineering Structures*, 27(4), 564-575. https://doi.org/10.1016/j.engstruct.2004.11.015

[22] M. Matallah, C. La Borderie and O. Maurel. (2010). A practical method to estimate crack openings in concrete structures. *International Journal for Numerical and Analytical Methods in Geomechanics*, 34(15), 1615-1633. https://doi.org/10.1002/nag.876

[23] M. Vassaux. (2015). Mechanical behaviour of quasi-brittle materials under cyclic loading: from numerical experimentation to structural analysis (in French). *Ph.D. thesis, Ecole Normale Supérieure de Cachan, LMT-Cachan, France.*